Effect of Reynolds Number and Periodic Unsteady Wake Flow Condition on Boundary Layer Development, Separation, and Intermittency Behavior Along the Suction Surface of a Low Pressure Turbine Blade

M. T. Schobeiri

B. Öztürk

Turbomachinery Performance and Flow Research Laboratory (TPFL), Texas A&M University, College Station, TX 77843-3123

David E. Ashpis

National Aeronautics and Space Administration, John H. Glenn Research Center at Lewis Field, Cleveland, OH 44135

The paper experimentally studies the effects of periodic unsteady wake flow and Reynolds number on boundary layer development, separation, reattachment, and the intermittency behavior along the suction surface of a low pressure turbine blade. Extensive unsteady boundary layer experiments were carried out at Reynolds numbers of 110,000 and 150,000 based on suction surface length and exit velocity. One steady and two different unsteady inlet flow conditions with the corresponding passing frequencies, wake velocities, and turbulence intensities were investigated. The analysis of the experimental data reveals details of boundary layer separation dynamics which is essential for understanding the physics of the separation phenomenon under periodic unsteady wake flow and different Reynolds numbers. To provide a complete picture of the transition process and separation dynamics, extensive intermittency analysis was conducted. Ensemble-averaged maximum and minimum intermittency functions were determined, leading to the relative intermittency function. In addition, the detailed intermittency analysis was aimed at answering the question as to whether the relative intermittency of a separated flow fulfills the universality criterion. [DOI: 10.1115/1.2219762]

Introduction

In recent years, gas turbine engine aerodynamicists have focused their attention on improving the efficiency and performance of the low pressure turbine (LPT) component. Research performed by the industry, research centers, and academia has shown that a reduction of the blade number can be achieved without substantially sacrificing the efficiency of the LPT blading. This reduction contributes to an increase in thrust/weight ratio, thus reducing the fuel consumption. Unlike the high pressure turbine that operates in a relatively high Reynolds number environment, the LPT of large commercial engines operates at Reynolds numbers ranging from 75,000 to 400,000. Since the major portion of the boundary layer, particularly along the suction surface, is laminar, the low Reynolds number, in conjunction with the local adverse pressure gradient, makes it susceptible to flow separation, thus increasing the complexity of the LPT boundary layer aerodynamics. The periodic unsteady nature of the incoming flow associated with wakes that originate from upstream blades substantially influences the boundary layer development, including the onset of the laminar separation, the extent of the separation bubble and its turbulent reattachment. Of particular relevance in the context of LPT aerodynamics is the interaction of the wake flow with the suction surface separation bubble. While the phenomenon of the unsteady boundary layer development and transition in the absence of the separation bubbles has been the subject of intensive research, the multiple effects of mutually interacting parameters on the LPT boundary layer separation and their physics still requires more research for full understanding.

The significance of the unsteady flow effect on efficiency and performance of compressor and turbine stages was recognized in the early seventies by several researchers. Fundamental research by Pfeil and Herbst [1], Pfeil et al. [2], and Orth [3], studied and quantified the effect of unsteady wake flow on the boundary layer transition along flat plates. Schobeiri and his coworkers [4–7] experimentally investigated the effects of the periodic unsteady wake flow and pressure gradient on boundary layer transition and heat transfer along the concave surface of a constant curvature plate. The measurements were systematically performed under different pressure gradients and unsteady wake frequencies using a squirrel cage type wake generator positioned upstream of the curved plate. Liu and Rodi [8] carried out the boundary layer and heat transfer measurements on a turbine cascade, which was installed downstream of a squirrel cage type wake generator, mentioned previously.

Analyzing the velocity and the turbulence structure of the impinging wakes and their interaction with the boundary layer, Chakka and Schobeiri [7] developed an intermittency-based unsteady boundary layer transition model. The analysis revealed a universal pattern for the relative intermittency function for all the frequencies and pressure gradients investigated. However, the above investigations were not sufficient to draw any conclusion with regard to an eventual universal character of the relative intermittency function. Further detailed investigations of the unsteady boundary layer on a high Reynolds number turbine cascade

Contributed by the International Gas Turbine Institute (IGTI) of ASME for publication in the JOURNAL OF TURBOMACHINERY. Manuscript received October 1, 2004; final manuscript received February 1, 2005. IGTI Review Chair: K. C. Hall. Paper presented at the ASME Turbo Expo 2005: Land, Sea and Air, Reno, NV, June 6–9, 2005, Paper No. GT2005-68600.

by Schobeiri et al. [9,10] and its subsequent analysis [11,12] verified the universal character of the relative intermittency function. For this purpose, Schobeiri et al. [9] utilized a conceptually different type wake generator, which is also used for the investigation presented in this paper. Fottner and his coworkers [13,14] and Schulte and Hodson [15] used the same wake generating concept for the investigations on the influence of the unsteady wake flow on the LPT-boundary layer. Kaszeta, Simon, and Ashpis [16] experimentally investigated the laminar-turbulent transition within a channel with the two curved walls resembling the suction and pressure surfaces of an LPT-blade using a retractable wake generator. Lou and Hourmouziadis [17] investigated the effect of oscillating inlet flow conditions on laminar boundary layer separation along a flat plate under LPT-pressure conditions. This was emulated by contouring the test section top wall. They studied the Reynolds number effect on the transition region. Their results showed that the higher Reynolds numbers cause an earlier transition and reduction of the transition length, while the separation point does not change its location.

Using the surface-mounted hot film measurement technique, Fottner and his coworkers [13,14], Schröder [18], and Haueisen, Hennecke, and Schröder [19] documented strong interaction between the wakes and the suction surface separation bubble on the LPT blades, both in the wind tunnel cascade tests and in a turbine rig. Furthermore, they investigated the boundary layer transition under the influence of the periodic wakes along the LPT surface and found that the interaction of the wake with the boundary layer greatly affects the loss generation. The investigations by Halstead et al. [20] on a large scale LP turbine use surface-mounted hot films to acquire detailed information about the quasi-shear stress directly on the blade surface. Investigations by Cardamone et al. [14] and Schröder [18] indicate that the benefit of the wake-boundary layer interaction can be used for the design procedure of modern gas turbine engines with a reduced LPT blade number, without altering the stage efficiency.

Most of the studies mentioned above on LP turbine cascade aerodynamics have largely concentrated on the measurement of the signals stemming from hot films mounted on the suction and pressure surfaces of the blades under investigation. Although this technique is qualitatively reflecting the interaction of the unsteady wake with the boundary layer, because of the lack of an appropriate calibration method, it is not capable of quantifying the surface properties such as the wall shear stress. The few boundary layer measurements are not comprehensive enough to provide any conclusive evidence for interpretation of the boundary layer transition and separation processes and their direct impact on profile loss, which is a critical parameter for blade design. Furthermore, the numerical simulation of the unsteady LPT blade aerodynamics, using conventional turbulence and transition models, fails if it is applied to low Reynolds number cases. Recent work presented by Cardamone et al. [14] shows that in the steady state case at Re =60,000 the separation is captured, however, for the unsteady case the separation bubble is not reproduced.

A recent experimental study by Schobeiri and Öztürk [21,22] investigated the physics of the inception, onset and extent of the separation bubble along a low pressure turbine blade, which was the first part of a series of investigations carried out at TPFL. A detailed experimental study on the behavior of the separation bubble on the suction surface of a highly loaded LPT blade under a periodic unsteady wake flow was presented in Ref. [21]. Surface pressure measurements were performed at Re=50,000, 75,000, 100,000, and 125,000. Increasing the Reynolds number has resulted in no major changes to the surface pressure distribution. They concluded that the unsteady wake flow, with its highly turbulent vortical core over the separation region, caused a periodic contraction and expansion of the separation bubble. It was proposed that, in conjunction with the pressure gradient and periodic wakes, the temporal gradient of the turbulence fluctuation, or more precisely the fluctuation acceleration $\partial \nu_{\text{rms}}/\partial t$, provides a higher momentum and energy transfer into the boundary layer, energizing the separation bubble and causing it to partially or entirely disappear. They found that for $\partial \nu_{\text{rms}}/\partial t > 0$ the separation bubble starts to contract, whereas for $\partial \nu_{\text{rms}}/\partial t < 0$ it gradually assumes the shape before the contraction. They argued that not only the existence of higher turbulence fluctuations expressed in terms of higher turbulence intensity influences the flow separation, but also its gradient is of crucial importance in suppressing or preventing the onset and the extent of the separation bubble. They stated that the fluctuation gradient is an inherent feature of the incoming periodic wake flow, and does not exist in a statistically steady flow that might have a high turbulence intensity. They also stated that unsteady wake flow, with its highly turbulent vortical core passing over the separation region, caused a periodic contraction and expansion of the separation bubble and a reduction of the separation bubble height. Increasing the passing frequency associated with a higher turbulence intensity further reduced the separation bubble height [21].

The objective of the present study, dealing with the specific issues of the LPT boundary layer aerodynamics, is to provide detailed unsteady boundary layer flow information to understand the underlying physics of the inception, onset, and extension of the separation bubble for different Reynolds numbers. Furthermore, the unsteady boundary layer data from the present and planned experimental investigations will serve to extend the intermittency unsteady boundary layer transition model developed by Schobeiri and his coworkers [7,11,12] to the LPT cases, where a separation occurs on the suction surface at a low Reynolds number at the design and off-design incidence. The experimental results are also intended to serve as benchmark data for a comparison with numerical computation using DNS or RANS codes.

It is well known that the boundary layer measurement is one of the most time consuming aerodynamic measurements. Any attempt to increase the number of parameters to be studied would inevitably result in a substantial increase of the measurement time. Considering this fact, the research facility described in Refs. [9,10], with state-of-the-art instrumentation, has been substantially modified to systematically and efficiently study the influence of the periodic unsteady and highly turbulent flow on the LPT cascade aerodynamics at the design and off-design incidence angles, where the Reynolds number, wake impingement frequency, free-stream turbulence, and the blade solidity can be varied independently.

Experimental Research Facility

To investigate the effect of unsteady wake flow on turbine and compressor cascade aerodynamics, particularly on unsteady boundary layer transition, a multipurpose, large-scale subsonic research facility was designed and has been taken into operation since 1993. Since the facility in its original configuration is described in Refs. [9,10,21], only a brief description of the modifications and the main components is given below. The research facility consists of a large centrifugal compressor, a diffuser, a settling chamber, a nozzle, an unsteady wake generator, and a turbine cascade test section as shown in Fig. 1. The compressor, with a volumetric flow rate of 15 m^3/s, is capable of generating a maximum mean velocity of 100 m/s at the test section inlet. The settling chamber consists of five screens and one honeycomb flow straightener to control the uniformity of the flow.

Two-dimensional periodic unsteady inlet flow is simulated by the translational motion of a wake generator (see Fig. 1), with a series of cylindrical rods attached to two parallel operating timing belts driven by an electric motor. To simulate the wake width and spacing that stem from the trailing edge of rotor blades, the diameter and number of rods can be varied. The rod diameter, its distance from the LPT blade leading edge, the wake width and the corresponding drag coefficient are chosen according to the criteria outlined by Schobeiri et al. [23]. The belt-pulley system is driven by an electric motor and a frequency controller. The wake-passing

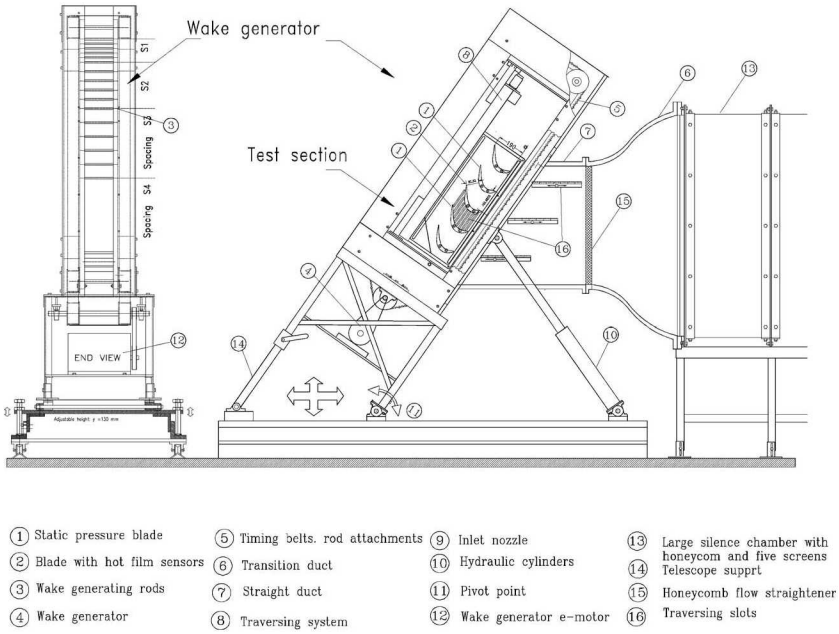

Fig. 1 Turbine cascade research facility with the components and the adjustable test section

frequency is monitored by a fiber-optic sensor. The sensor also serves as the triggering mechanism for data transfer and its initialization, which is required for ensemble-averaging. This type of wake generator produces clean, two-dimensional wakes, whose turbulence structure, decay and development are, to a great extent, predictable [23]. The unsteady boundary layer transition and heat transfer investigations [9–12] performed on this facility serve as the benchmark data for validation of turbulence models, transition models and general code assessments.

To account for a high flow deflection of the LPT cascade, the entire wake generator and test section unit, including the traversing system, was modified to allow a precise angle adjustment of the cascade relative to the incoming flow. This is done by a hydraulic platform, which simultaneously lifts and rotates the wake generator and test section unit. The unit is then attached to the tunnel exit nozzle with an angular accuracy less than 0.05 deg, which is measured electronically.

The special design of the facility and the length of the belts (L_{belt}=4960 mm) enable a considerable reduction of the measurement time. For the present investigation, two clusters of rods with constant diameters of d=2 mm are attached to the belts as shown in Fig. 2. The two clusters, with spacings S_R=160 mm and S_R =80 mm, are separated by a distance which does not have any rods, thus simulating steady state case (S_R=∞). Thus, it is possible to measure sequentially the effect of three different spacings at a single boundary layer point. To clearly define the influence domain of each individual cluster with the other one, the clusters are arranged with a certain distance between each other. Using the triggering system mentioned above and a continuous data acquisition, the buffer zones between the data clusters are clearly visible.

The data analysis program cuts the buffer zones and evaluates the data pertaining to each cluster. Comprehensive preliminary measurements were carried out to make sure that the data were exactly identical to those when the entire belt length was attached with rods of constant spacing, which corresponded to each individual cluster spacing. The cascade test section shown in Fig. 1, located downstream of the wake generator, includes five LPT blades with a height of 200.0 mm and the chord of 203.44 mm. For boundary layer investigations, five identical "Pak B" airfoils designed by Pratt & Whitney were implemented and whose cascade geometry is given in Table 1.

The blade geometry resembles the essential feature, such as the laminar boundary layer separation, that is inherent to typical LPT blades. The blade geometry was made available to NASA researchers and academia to study the specific problems of LPT flow separation, its passive and active control and its prevention. As shown in Ref. [9], this blade number is necessary and sufficient to secure a spatial periodicity for the cascade flow. Identical pressure distributions taken from blade Nos. 2 and 4 (counted from the test section bottom, Fig. 1) demonstrate the required periodicity. These blades were specially manufactured for measurement of pressure and showed identical pressure distributions.

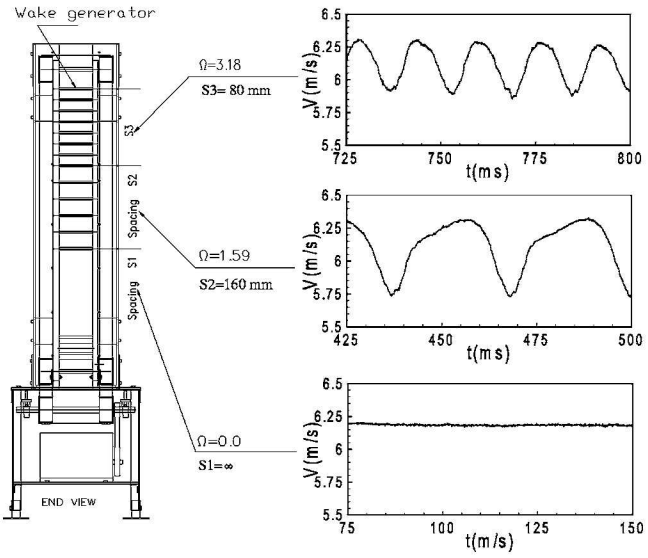

Fig. 2 Wake generator

Table 1 Parameters of turbine cascade test section

Parameters	Values	Parameters	Values
Inlet velocity	V_{in}=4 m/s	Inlet turbulence intensity	Tu_{in}=1.9%
Rod translational speed	U=5.0 m/s	Blade Re number	Re=110,000
Nozzle width	W=200.0 mm	Blade height	h_B=200 mm
Blade chord	c=203.44 mm	Cascade solidity	σ=1.248
Blade axial chord	c_{ax}=182.85 mm	Zweifel coefficient	Ψ_A=1.254
Blade suction surface length	L_{SS}=270.32 mm	Cascade angle	γ=55 deg
Cascade flow coefficient	ϕ=0.80	Cascade spacing	S_B=163 mm
Inlet air angle to the cascade	α_1=0 deg	Exit air angle from the cascade	α_2=90 deg
Rod diameter	D_R=2.0 mm	Rod distance to lead. edge	L_R=122 mm
Cluster 1 (no rod, steady)	S_R=4 ∞	Ω— parameter steady case	Ω=0.0
Cluster 2 rod spacing	S_R=160.0 mm	Ω— parameter for cluster 1	Ω=1.59
Cluster 3 rod spacing	S_R=80.0 mm	Ω— parameter for cluster 2	Ω=3.18

A computer-controlled three-axes traversing system (Fig. 3) is used to measure the inlet velocities, turbulence intensity, and the entire boundary layer distribution on suction and pressure surfaces. The traversing system was added very recently to the test section to allow the probe to reach all streamwise positions along the suction and pressure surfaces, with a positioning accuracy of 1 μm. The three-axis system is vertically mounted on the plexiglass side wall. Each axis is connected to a direct current-stepper motor with an encoder and decoder. The optical encoder provides a continuous feedback to the stepper motor for accurate positioning of the probes. The x- and y-axis of the system are capable of traversing along the suction and pressure surfaces in small steps up to 1 μm. The third axis rotates the probe holder with an angular accuracy less then $\Delta\Theta$=0.05 deg, which is specifically required for boundary layer investigations where the measurement of the laminar sublayer is of particular interest.

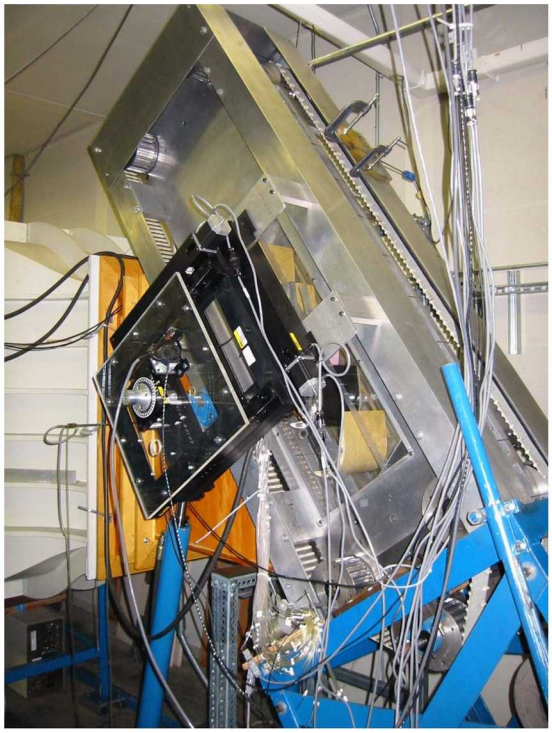

Fig. 3 Turbine cascade research facility with three-axis traversing system

Instrumentation, Data Acquisition, and Data Reduction

The data acquisition system is controlled by a personal computer that includes a 16-channel, 12-bit analog-digital (A/D) board. Time-dependent velocity signals are obtained by using a commercial three-channel, constant temperature hot wire anemometer system that has a signal conditioner with a variable low pass filter and adjustable gain. A hot wire probe placed upstream of the diffuser monitors the reference velocity at a fixed location. The pneumatic probes are connected to high precision differential pressure transducers for digital readout. Several calibrated thermocouples are placed downstream of the test section to constantly monitor the flow temperature. The wake generator speed and the passing frequency signals of the rods are transmitted by a fiber-optic trigger sensor. The passage signals of the rods are detected by the sensor using a silver-coated reflective paint on one of the belts. This sensor gives an accurate readout of the speed of the wake generator and the passing frequency of the rods. The signals of the pressure transducers, thermocouples and trigger sensors are transmitted to the A/D board and are sampled by the computer. To ensure the cascade periodicity, the second and fourth blades are each instrumented with 48 static pressure taps. Two adjacent blades are used for boundary layer measurement. The taps are connected to a scanivalve, which sequentially transfers the pressure signals to one of the transducers connected to the A/D board.

The unsteady data are taken by calibrated, custom designed miniature single hot wire probes. At each boundary layer position, samples were taken at a rate of 20 kHz for each 100 revolutions of the wake generator. The data were ensemble averaged with respect to the rotational period of the wake generator. Before final data were taken, the number of samples per revolution and the total number of revolutions were varied to determine the optimum settings for convergence of the ensemble average.

For the steady state case, the instantaneous velocity components are calculated from the temperature-compensated instantaneous voltages by using the calibration coefficients. The instantaneous velocity can be represented in the following form:

$$V = \bar{V} + \nu \tag{1}$$

where $\bar{V}$ is the mean (time-averaged) velocity and ν is the turbulent fluctuation component. The mean velocity, also known as the time average, is given by

$$\bar{V} = \frac{1}{M}\sum_{j=1}^{M} V_j \tag{2}$$

where M is the total number of samples at one boundary layer location. The root mean square value of the turbulent velocity fluctuation is

$$\nu = \sqrt{\frac{1}{M}\sum_{j=1}^{M}(V_j - \bar{V})^2} \tag{3}$$

and the local turbulence intensity is defined as:

$$\mathrm{Tu_{luc}} = \frac{\nu}{\bar{V}} \times 100 = \frac{1}{\bar{V}}\sqrt{\frac{1}{M}\sum_{j=1}^{M}(V_j - \bar{V})^2} \times 100 \tag{4}$$

For unsteady cases, the ensemble-averaged velocity, fluctuation velocity, and the turbulence intensity were calculated from the instantaneous velocity samples by:

$$V_i(t_i) \equiv \langle V_i(t_i)\rangle = \frac{1}{N}\sum_{j=1}^{N} V_{ij}(t_i) \tag{5}$$

$$\nu_i(t_i) \equiv \langle \nu_i(t_i)\rangle = \sqrt{\frac{1}{N}\sum_{j=1}^{N}[V_{ij}(t_i) - \langle V_i(t_i)\rangle]^2} \tag{6}$$

$$\mathrm{Tu}_i(t_i) \equiv \langle \mathrm{Tu}_i(t_i)\rangle = \frac{\langle \nu_i(t_i)\rangle}{\langle V_i(t_i)\rangle} \times 100 \tag{7}$$

where $N=100$ is the total number of wake generator periods and M is the number of samples taken per period. $\langle V_i(t_i)\rangle$ is the ensemble-averaged velocity for the particular boundary layer traverse.

Experimental Results and Discussion

Detailed surface pressure and boundary layer measurements were performed at Reynolds numbers of 110,000 and 150,000. These Reynolds numbers, which pertain to a typical cruise operation, exhibit a representative value within LPT operating range between 75,000 and 400,000, as discussed by Hourmouziadis [24]. Furthermore, it produces separation bubbles that can be accurately measured by miniature hot wire probes. For the Reynolds numbers of 110,000 and 150,000, three different reduced frequencies were examined. To generate unsteady wakes, cylindrical rods with the diameter $d_R=2$ mm were chosen to fulfill the similar criterion that requires the generation of a drag coefficient, C_D, that is approximately equal to the C_D of the turbine blade with the chord and spacing given in Table 1 (for details we refer to the studies in Refs. [23,25]). Furthermore, we define a reduced frequency Ω that includes the cascade solidity σ, the flow coefficient φ, the blade spacing S_B, and the rod spacing S_R. The reduced frequency Ω is an extension of Strouhal number, in the sense that it incorporates the rod spacing S_R and the blade spacing S_B in addition to the inlet velocity and wake generator speed. For surface pressure measurement, rods with uniform spacing as specified in Table 1 were attached over the entire belt length. For boundary layer measurement, however, clusters of rods were attached, as mentioned previously.

Surface Pressure Distributions. Detailed pneumatic surface pressure measurements were taken at Re=110,000 and 150,000. For each Reynolds number, three different reduced frequencies, namely $\Omega=0.0$, 1.59, and 3.18, are applied that correspond to the rod spacings $S_R=\infty$ (no rod), 160, and 80 mm. The pressure distributions in Fig. 4 show the results of the steady case and two unsteady cases. The pressure signals inherently signify the time-averaged pressure, because of the internal pneumatic damping effect of the connecting pipes to the transducer. The noticeable deviation in pressure distribution between the steady and unsteady cases, especially on the suction surface, is due to the drag forces caused by the moving rods. The drag forces are imposed on the main stream and cause momentum deficiency that leads to a reduction of the total and static pressure. The time-averaged pressure coefficients along the pressure and suction surfaces are plotted in Fig. 4. The suction surface (upper portion) exhibits a strong

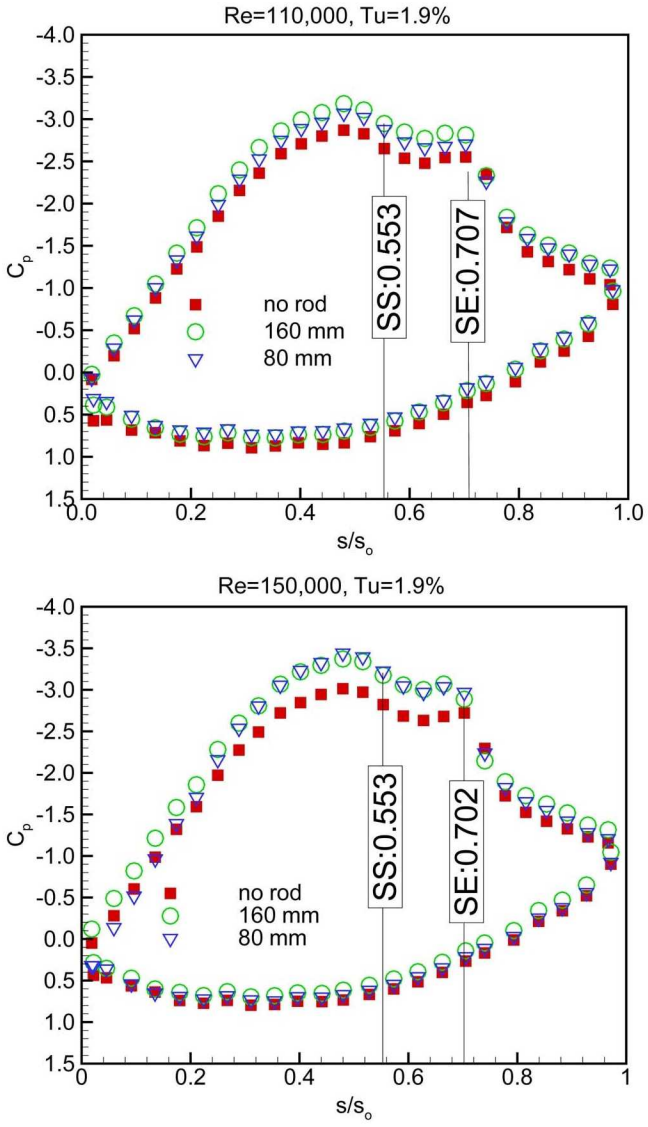

Fig. 4 Static pressure distributions at two different Re numbers and reduced frequencies Ω=0, 1.59, 3.18 (no rod, 160, 80 mm), SS=separation start, SE=separation end

negative pressure gradient. The flow accelerates at a relatively steep rate and reaches its maximum surface velocity that corresponds to the minimum $C_p=-3.5$ at $s/s_0=0.42$. Passing through the minimum pressure, the fluid particles within the boundary layer encounter a positive pressure gradient that causes a sharp deceleration up to $s/s_0=0.55$. This point signifies the beginning of the laminar boundary layer separation and the onset of a separation bubble. As seen in the subsequent boundary layer discussion, the separation bubble characterized by a constant C_p plateau extends up to $s/s_0\approx0.74$, thus occupying more than 19% of the suction surface and constituting a large separation. Passing the plateau, the flow first experiences a second sharp deceleration indicative of a process of reattachment, followed by a further deceleration at a moderate rate. On the pressure surface, the flow accelerates at a very slow rate, reaches a minimum pressure coefficient at $s/s_0=0.42$, and continues to accelerate until the trailing edge has been reached. Unlike the suction surface, the pressure surface boundary layer does not encounter any adverse positive pressure gradient that triggers separation. However, close to the leading edge, a small plateau extending from $s/s_0=0.08-0.16$ indicates the existence of a small size separation bubble that might be attributed to a minor inlet flow incidence angle.

Considering the unsteady case with the reduced frequency $\Omega=1.59$ corresponding to a rod spacing of $S_R=160$ mm, Fig. 4 exhibits a slight difference in the pressure distribution between the steady and unsteady cases. As mentioned above, this deviation is attributed to the momentum deficiency that leads to a reduction of the total and static pressure. For Re=110,000, the wakes have a reducing impact on the streamwise extent of the separation plateau. As seen in Fig. 4(*a*), the trailing edge of the plateau has shifted from $s/s_0=0.74$ to $s/s_0=0.702$. This shift reduced the streamwise extent of the separation plateau from 19% to 15% of the suction surface length which is, in this particular case, 21% of reduction in streamwise extent of the separation. Increasing the reduced frequency to $\Omega=3.18$ by reducing the rod spacing to $S_R=80$ mm causes a slight shift of the C_p distribution compared with $\Omega=1.59$ case. One should bear in mind that pneumatically measured surface pressure distribution represents a time integral of the pressure events only.

Increasing the Reynolds number to Re=150,000 has not brought major changes in steady state C_p distribution. However, the combination of higher Reynolds number with unsteady wakes reveals the noticeable deviation on the streamwise extent of the separation plateau. As seen in Fig. 4(*b*), the trailing edge of the plateau has shifted from $s/s_0=0.74$ to $s/s_0=0.702$ for Reynolds number of 150,000. The combination of higher Reynolds number with high unsteady wakes introduce fluctuation kinetic energy into the boundary layer which tends to inhibit the separation tendency. C_p distribution clearly shows that the wake impingement with higher Reynolds number shortens the streamwise extent of the separation zone compared to the steady case.

Detailed information regarding the structure of the separation bubble is delivered by means of a detailed unsteady boundary layer measurement using hot wire probes, as will be discussed in the subsequent sections.

Time Averaged Velocity and Fluctuation Distributions. Following the surface pressure investigations that mainly addressed the onset and extent of the separation zone discussed previously, comprehensive boundary layer measurements were performed to identify the streamwise and normal extent, as well as the deformation of the separation zone under unsteady wake flow. The steady state case serves as the reference configuration.

Consistent with the surface pressure distribution above, the effect of the wake frequency on the time-averaged velocity profiles and fluctuation velocity distribution are presented for one steady and two unsteady inlet flow conditions on the suction surface along 31 streamwise locations for the Reynolds number of 110,000, and 41 streamwise locations for the Reynolds number of 150,000. After completing the velocity measurements, the boundary layer coordinates were transformed into a blade orthogonal coordinate system. Velocities at blade normal positions were obtained by interpolating their transformed values. The results showed almost no difference between the interpolated and noninterpolated velocity data. Experimental investigations were performed for three different values of $\Omega=0.0$, 1.59, and 3.18. These values cover the reduced frequency range encountered in LPT design and off-design operation conditions.

The effect of wake frequency on time-averaged velocity and velocity fluctuation distributions is shown in Figs. 5–8 at six representative streamwise locations for Re=110,000 and Re=150,000. Among 31 streamwise positions measured along the suction surface, Figs. 5 and 6 display the velocity and fluctuation distributions at one streamwise position upstream, three positions within and two positions downstream of the separation bubble. The diagrams include the steady state data for reference purposes, $\Omega=0.0$ ($S_R=\infty$), unsteady data for $\Omega=1.59$ ($S_R=160$ mm) and $\Omega=3.18$ ($S_R=80$ mm).

As Fig. 5 indicates, in the upstream region of the separation bubble the flow is fully attached. At $s/s_0=0.49$, the velocity distributions inside and outside the boundary layer experience a hardly noticeable decrease with increasing the reduced frequency. At the same positions, however, the time-averaged velocity fluctuations shown in Fig. 6 exhibit substantial changes within the

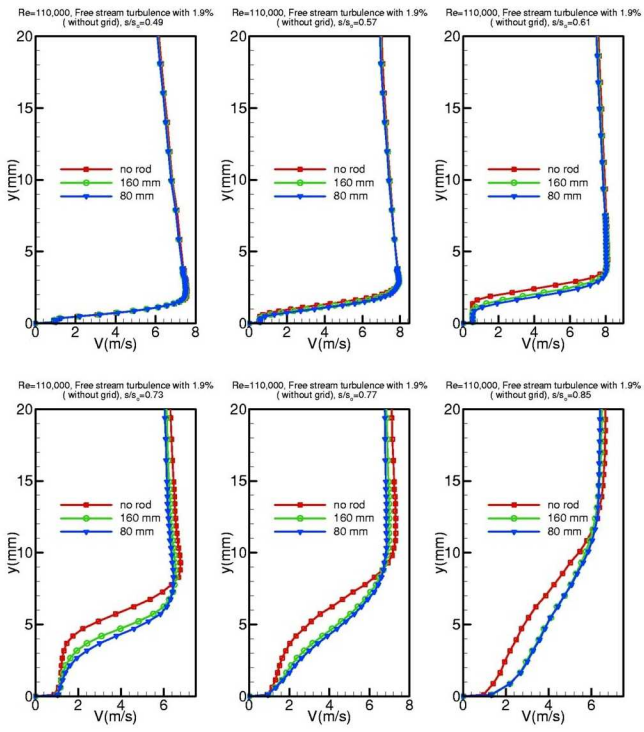

Fig. 5 Distribution of time-averaged velocities along the suction surface for steady case $\Omega=0$ ($S_R=\infty$) and unsteady cases $\Omega=1.59$ ($S_R=160$ mm) and $\Omega=3.18$ ($S_R=80$ mm) at Re=110,000

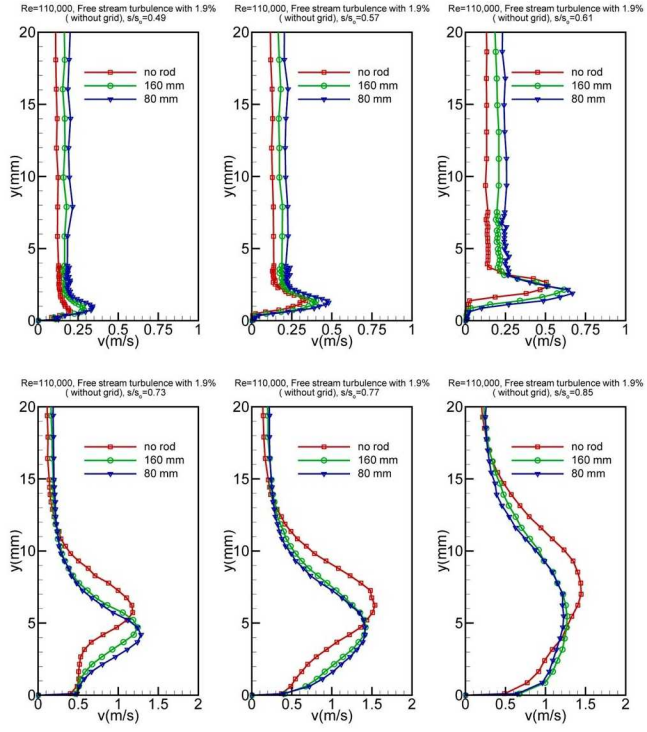

Fig. 6 Distribution of time-averaged velocity fluctuations along the suction surface for steady case $\Omega=0$ ($S_R=\infty$) and unsteady cases $\Omega=1.59$ ($S_R=160$ mm) and $\Omega=3.18$ ($S_R=80$ mm) at Re=110,000

boundary layer, as well as outside it. The introduction of the periodic unsteady wakes with highly turbulent vortical cores and the subsequent mixing has systematically increased the free-stream turbulence level from 1.9% in steady case to almost 3% for Ω =3.18 (S_R=80 mm). Comparing the unsteady cases, Ω=1.59 and 3.18, with the steady reference case, Ω=0.0, indicates that with increasing Ω the lateral position of the maximum velocity fluctuation shifts away from the wall. This is due to the periodic disturbance of the stable laminar boundary layer upstream of the separation bubble.

As Fig. 6 shows, a substantial influence of the wake frequency is observed inside the separation bubble at s/s_0=0.57, s/s_0 =0.61, and s/s_0=0.73. The wake impingement introduces fluctuation kinetic energy stemming from its vortical core into the boundary layer, trying to energize it and to reverse the separation tendency. As seen from the velocity profiles, the wake frequency effect shortens the bubble height and reduces its streamwise extent. Compared to the steady case, however, the onset of the separation bubble has not changed substantially. This shows that, although the impingement of the vortical wake core periodically reduces the separation bubble height, it does not have sufficient momentum to completely suppress it. Figure 6 displays the details of the turbulence fluctuation activities in and outside of the separation bubble at s/s_o=0.57, s/s_o=0.61, and s/s_o=0.73. Strong turbulent activities are measured within the separation bubble that extends to the shear layer. Outside the separation bubble, the turbulence activities rapidly decrease, approaching the free-stream levels that correspond to the individual unsteady frequency discussed above. A comparison of the unsteady cases, Ω=1.59 and 3.18, with the steady reference case, Ω=0.0, indicates that with increasing Ω the lateral position of the maximum fluctuation shifts toward the wall. This is the consequence of the overall decrease of the lateral extension of the separation bubble as a result of wake impingement.

Close to the bubble trailing edge at s/s_o=0.73 and s/s_o=0.77, Fig. 5 shows that the undisturbed flow, Ω=0 (S_R=∞), still has its inflectional pattern. The perturbation by impinging the wakes causes the velocity profile to become fully turbulent and attached. Once the profile becomes fully turbulent, increasing the reduced frequency from Ω=1.59 (S_R=160 mm) to Ω=3.18 (S_R=80 mm) does not substantially change the velocity distribution pattern. Figure 6 displays the details of the velocity fluctuation activities inside and outside of the reattached boundary layer at s/s_o=0.77 and s/s_o=0.85. As in Fig. 5, once the velocity profile has become fully turbulent, its corresponding fluctuation distribution remains almost unchanged.

In the context of transitional and turbulent boundary layer flow investigations, it is worth noting the different behavior of these boundary layer types. According to the previous investigations by Schobeiri et al. [10–12] in a HP-turbine cascade with transitional boundary layer throughout, an increased wake frequency causes turbulence fluctuations to rise inside and outside the boundary layer. However, in the LPT case with the boundary layer separation, once the boundary layer is reattached and the velocity distribution assumes a fully turbulent profile, no major changes are observed either in the velocity or in the fluctuation velocity distribution.

For Re=150,000, Figs. 7 and 8 display the velocity and velocity fluctuation distributions at the same streamwise locations as discussed above. Likewise, the diagrams include the steady state, Ω=0.0, data for reference purposes and the unsteady data for Ω =1.59 and Ω=3.18. Although the results for Re=150,000 show very similar velocity and fluctuation patterns, it is observed that the starting point of the separation bubble and its reattachment point have moved slightly further downstream. This is clearly visible in Fig. 7, at s/s_o=0.73 and s/s_o=0.77, where the inflectional pattern of the velocity profiles indicates that the above streamwise positions are located close to the trailing edge within the separation bubble. Increasing the frequency from Ω=0 (S_R=∞) to Ω =3.18 (S_R=80 mm) brings the profiles closer to the fully turbulent pattern, without collapsing. The same statement is true for the turbulence fluctuations, Fig. 8, at s/s_o=0.73 and s/s_o=0.77. Also,

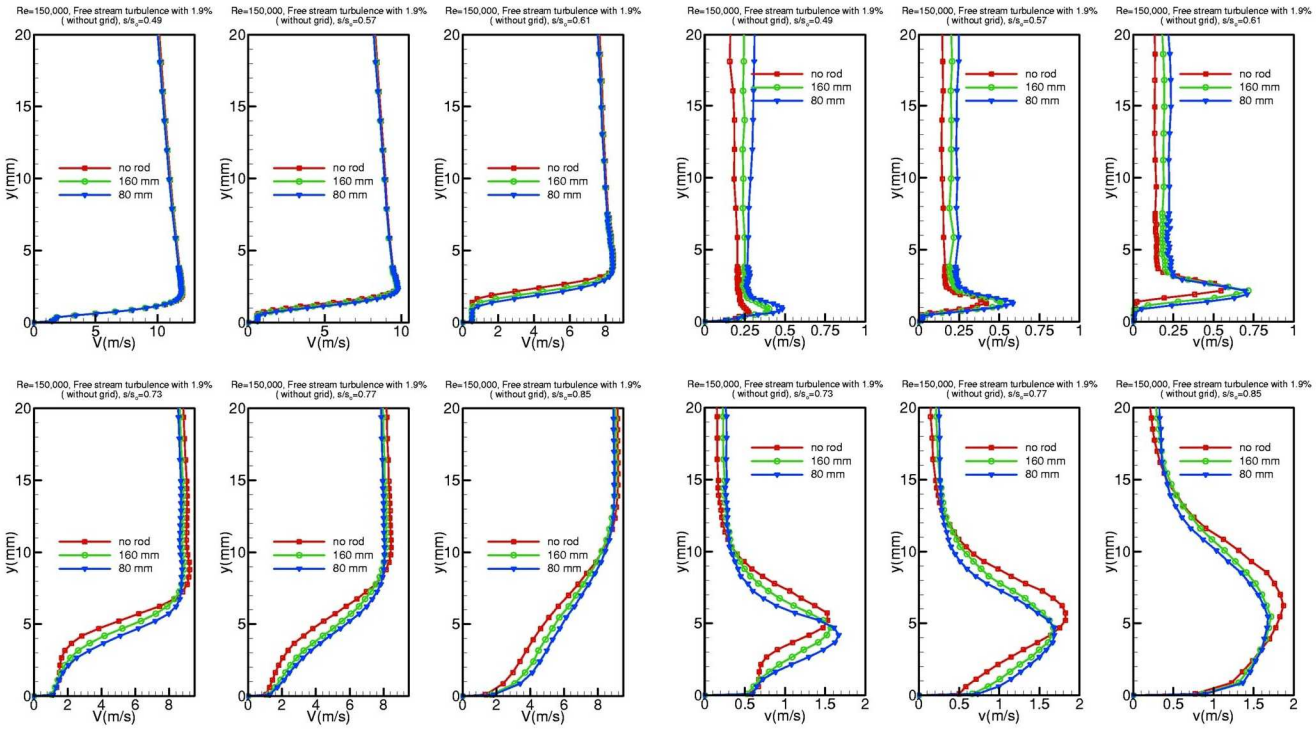

Fig. 7 Distribution of time-averaged velocity distributions along the suction surface for steady case Ω=0 (S_R=∞) and unsteady cases Ω=1.59 (S_R=160 mm) and Ω=3.18 (S_R =80 mm) at Re=150,000

Fig. 8 Distribution of time-averaged fluctuation velocities along the suction surface for steady case Ω=0 (S_R=∞) and unsteady cases Ω=1.59 (S_R=160 mm) and Ω=3.18 (S_R =80 mm) at Re=150,000

the size of the separation bubble is smaller when compared to that for Re=110,000. To achieve a noticeable impact of the Reynolds number on the onset and extent of the bubble, the Reynolds number needed to increase above 150,000.

Temporal Behavior of the Separation Zone Under Periodic Unsteady Wake Flow. Velocity distributions on the suction surface with time as the parameter are plotted in Figs. 9–12 for Re =110,000, 150,000 for rod spacings S_R=80 mm and S_R =160 mm that correspond to Ω=1.59 and 3.18. The nondimensional time (t/τ) values are chosen that they represent the temporal states within one full period of wake passing. For Re =110,000, Figs. 9(*a*)–9(*f*) show the velocity distributions, inside and outside the boundary layer at fixed s/s_o locations, experience moderate to pronounced changes. Figure 9(*a*) represents the instantaneous velocity distribution upstream of the separation zone, followed by Figs. 9(*b*)–9(*f*) which represent the velocity distributions inside the separation zone. In discussing the following results, we simultaneously refer to the wake distribution as well as the turbulence fluctuation results.

Figure 9(*a*) exhibits the velocity distribution on the suction surface at s/s_o=0.49. At this streamwise position, the laminar boundary layer is subjected to a strong negative pressure gradient. The velocity distributions at different (t/τ) experience changes in magnitude that reflect the corresponding changes of the impinging periodic wake velocity. It is worth noting that, despite the injection of turbulence kinetic energy by the impinging wakes, no local instantaneous boundary layer transition occurs. This is because of the strong negative pressure gradient that prevents the boundary layer from becoming instantaneously transitional. Instantaneous velocity distributions inside the separation zone are shown in Figs. 9(*b*)–9(*f*).

As a representative case, we discuss the results plotted in Fig. 9(*e*) at s/s_o=0.65. During the time interval from t/τ close to 0.5 (1.5, 2.5, etc.) to about t/τ=0.75 (1.75, 2.75, etc.), the separation zone is exposed to the wake external flow with relatively lower turbulence level. This flow does not have the capability to suppress the separation zone. Thus, the separation region is clearly shown by the velocity distributions at t/τ=0.5 and t/τ=0.75. As the wake passes over the blade at s/s_o=0.65 introducing high turbulence kinetic energy into the boundary layer, the boundary layer is energized, causing the separation zone to partially reduce. To emphasize this statement, the steady state velocity distribution at the same streamwise position is also plotted in Fig. 9(*e*) using full circles. It shows clearly the separated nature of the boundary layer which coincides with the instantaneous velocity profile at t/τ=0.75. Intermediate times reflect the gradual change between different t/τ states as the flow is undergoing the influence of the oncoming wake. Moving to the trailing edge of the separation zone, at s/s_o=0.73, Fig. 9(*f*), a partial reduction in boundary layer thickness as the result of wake impingement is visible, however, the separation zone does not seem to disappear.

Figures 10(*a*)–10(*f*) show that the velocity distributions outside the boundary layer at fixed s/s_o locations experience noticeable changes at Ω=3.18 (S_R=80 mm). Increasing the wake passing frequency causes the wake turbulence kinetic energy to increase, resulting in a stronger suppression compared with the Ω=1.59 (S_R=160 mm) case. As seen in Figs. 11 and 12, increasing the Reynolds number to 150,000 causes the leading and trailing edges of the separation bubble to move further downstream. It is also observed that increasing the Reynolds number reduces the size of the separation bubble.

The effect of the periodic unsteady wakes on the onset and extent of the separation bubble is shown in Figs. 13–16 for Re =110,000 and 150,000, and for two different frequencies, namely Ω=1.59 and Ω=3.18. These figures display the full extent of the separation bubble and its behavior under a periodic wake flow impingement at different t/τ. The wake propagation for Ω=1.59 and Ω=3.18 is analyzed and the value of t/τ corresponds to the point in the cycle at which the data acquisition system is triggered. During a rod passing period, the wake flow and the separation bubble undergo a sequence of flow states which are not noticeably

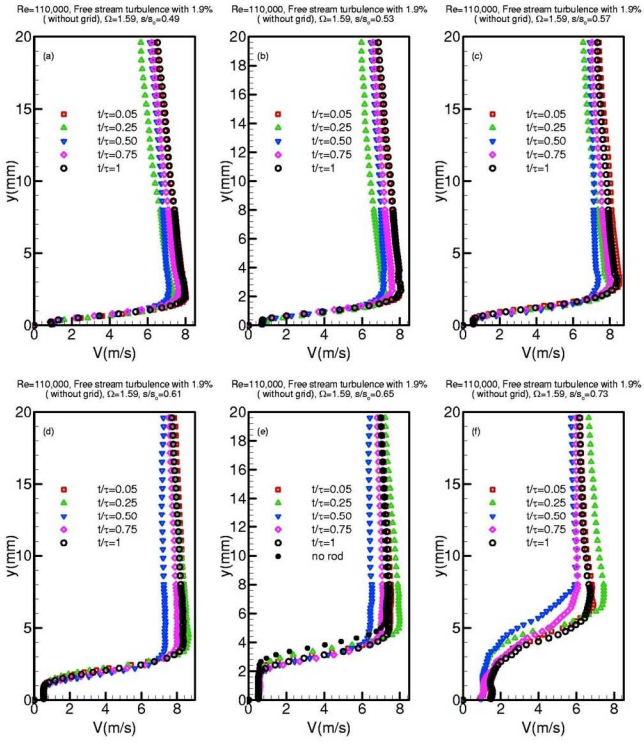

Fig. 9 Distribution of the ensemble-averaged velocity development along the suction surface for different s/s_0 with time t/τ as parameter for Ω=1.59 (S_R=160 mm) and Re=110,000

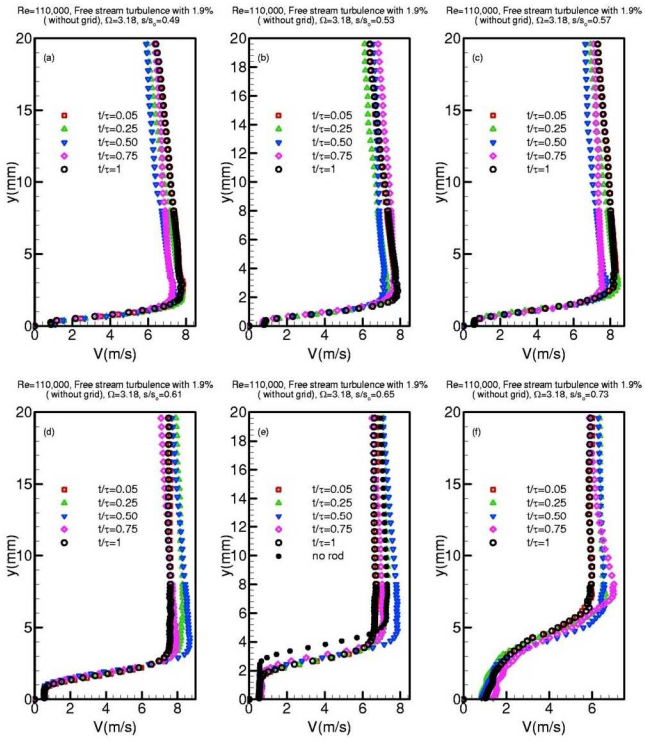

Fig. 10 Distribution of the ensemble-averaged velocity development along the suction surface for different s/s_0 with time t/τ as parameter for Ω=3.18 (S_R=80 mm) and Re=110,000

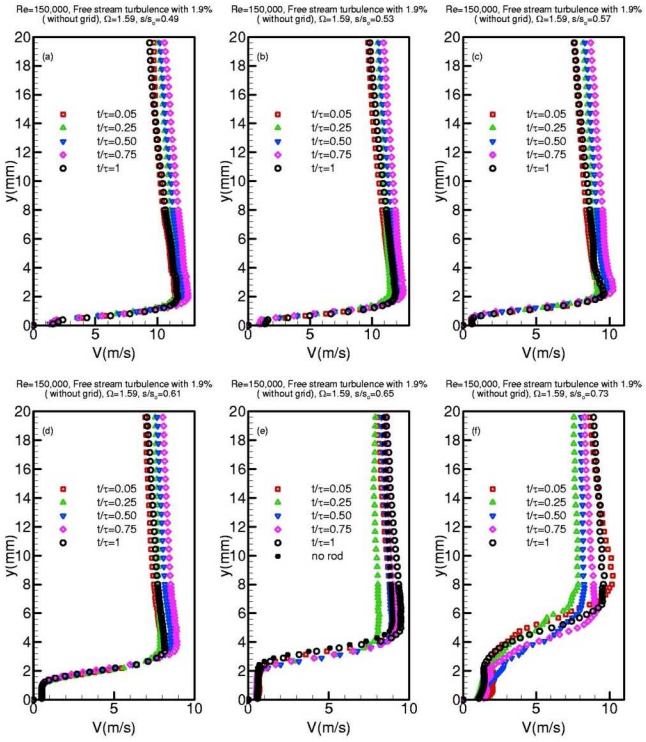

Fig. 11 Distribution of the ensemble-averaged velocity development along the suction surface for different s/s_0 with time t/τ as parameter for Ω=1.59 (S_R=160 mm) and Re=150,000

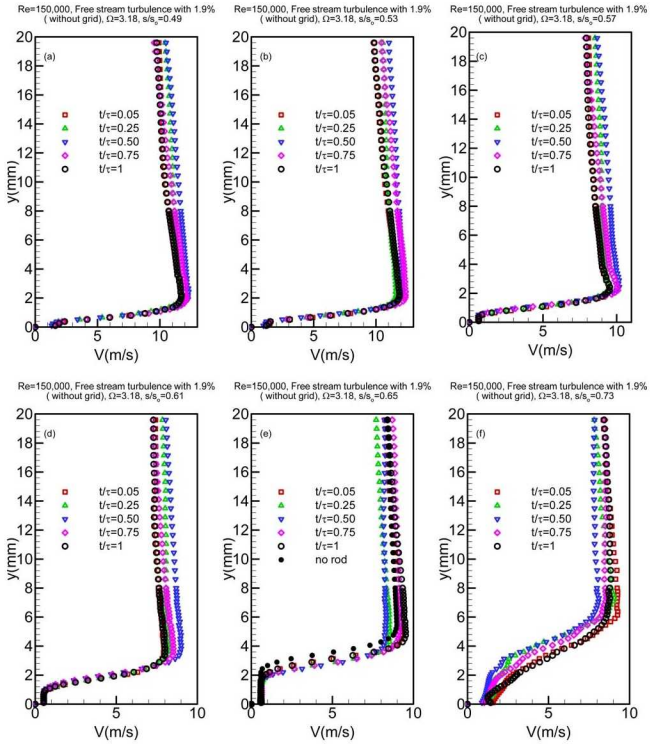

Fig. 12 Distribution of the ensemble-averaged velocity development along the suction surface for different s/s_0 with time t/τ as parameter for Ω=3.18 (S_R=80 mm) and Re=150,000

different when the unsteady data are time averaged.

Starting with Re=100,000 and Ω=1.59, Fig. 13(*a*) exhibits the separation bubble in its full size at t/τ=0.25. At this instant of time, the incoming wakes have not reached the separation bubble. At t/τ=0.5, the wake, with its highly turbulent vortical core, passes over the blade and generates high turbulence kinetic energy. At this point, the wake turbulence penetrates into the bubble causing a strong mass, momentum, and energy exchange between the wake flow and the fluid contained within the bubble. This exchange causes a dynamic suppression and a subsequent contraction of the bubble. As the wake travels over the bubble, the size of the bubble continues to contract at t/τ=0.75 and reaches its minimum size at t/τ=1.0. At t/τ=1, the full effect of the wake on the boundary layer can be seen before another wake appears and the bubble moves back to the original position. Similar results are observed when operating at the same Reynolds number, Re =110,000, but at a higher reduced frequency, Ω=3.18, Figs. 14(*a*)–14(*d*). A comparison of Figs. 14(*a*)–14(*d*) with Figs. 12(*a*)–12(*d*) illustrates the pronounced influence of higher reduced frequency which causes more frequent penetration of wake turbulence into the separation bubble, causing a stronger suppression and subsequent contraction of the bubble.

Figures 15 and 16 display the behavior of the separation bubble under higher Reynolds number, Re=150,000, and reduced frequencies, Ω=1.59 and Ω=3.18. While the higher Reynolds number moves the separation bubble further downstream. Similar contracting effects as discussed above are observed at Ω=1.59. However, doubling the reduced frequency and increasing the Reynolds number is associated with the higher turbulence intensity that leads to stronger suppression of the separation bubble, as shown in Figs. 15 and 16.

Intermittency Analysis

Intermittency distribution, which identifies whether the flow is laminar or turbulent inside the boundary layer, is calculated following the method of Hedley and Keffer [26]. Instantaneous velocity is sensitized to increase its discriminatory capabilities between turbulent and nonturbulent parts of the signal. For this purpose, the multiplication of the first derivative of the velocity signal and the velocity signal is used for further analysis. This is called the detector function, $S(t)$, defined as

$$S(t) = \left| u\frac{\partial u}{\partial t} \right| \tag{8}$$

The above detector function is used by many researchers, including Antonia and Bradshaw [27], Kovasznay et al. [28], Bradshaw and Murlis [29], and Schobeiri and his coworkers [7,12]. A very recent paper by Schobeiri [30] extensively discusses different issues relative to intermittency based transition modeling. Though sensitized detector function separates the turbulent and nonturbulent zones of the fluid, there is still some overlap between the two near the origins. The discrimination between the two zones of the flow will be ideal when the overlap between the two distributions is minimal or zero. To eliminate the disturbing effects of the velocity signal peaks, a smoothing procedure is applied to the $S(t)$ signal. The mean value of ten consecutive $S(t)$ values is calculated and the ten values are substituted by their mean value of $S_{sm}(t)$. After smoothing the detector function, a threshold level C is then applied to the smoothed detector function to distinguish between true turbulence and the signal *noise*. It is defined as

$$I(t) = \begin{cases} 1 \text{ when } S_{sm}(t) \geq C \\ 0 \text{ when } S_{sm}(t) < C \end{cases} \tag{9}$$

Once the threshold level is applied to the detector function $S(t)$, the result is a random square wave called the indicator function I, with 0's representing the nonturbulent case and 1's indicating the turbulent behavior of the boundary layer. A threshold level, C, of 1.2 is used for all the data on the suction surface. In the absence of length scales, this value is chosen from visual observations. Several other values of C are tested and little qualitative difference is seen in the intermittency distribution during transition. Though the

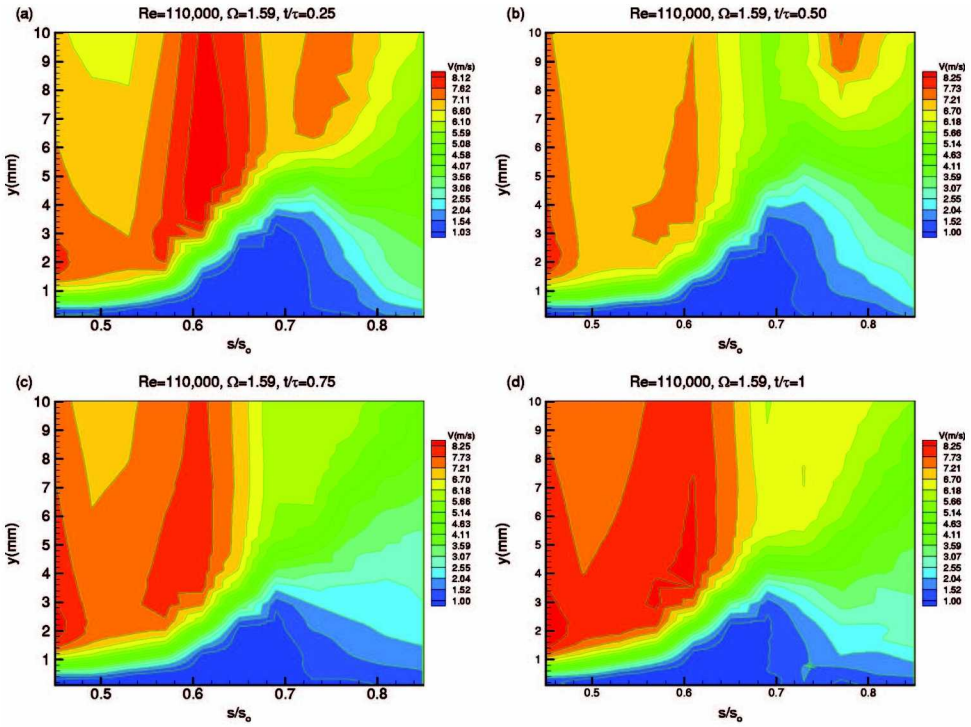

Fig. 13 Ensemble-averaged velocity contours along the suction surface for different s/s_0 with time t/τ as parameter for Ω=1.59 (S_R=160 mm), Re=110,000

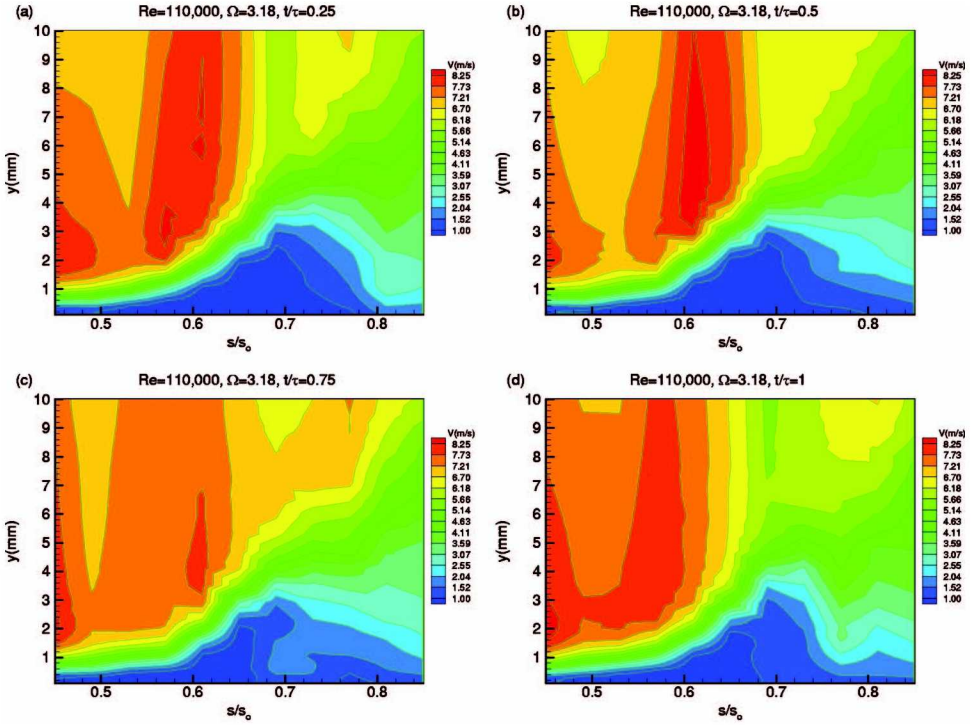

Fig. 14 Ensemble-averaged velocity contours along the suction surface for different s/s_0 with time t/τ as parameter for Ω=3.18 (S_R=80 mm), Re=110,000

intermittency values vary with different values of C, the important parameters like start and end of transition are not affected by C. The resulting square wave after applying the threshold is ensemble averaged to get the ensemble-averaged intermittency as follows

$$\langle \gamma_i(t_i) \rangle = \frac{1}{N} \sum_{j=1}^{N} I_{ij}(t_i) \tag{10}$$

where N is the number of revolutions of the wake generator for which the data are collected. For time-averaged intermittency,

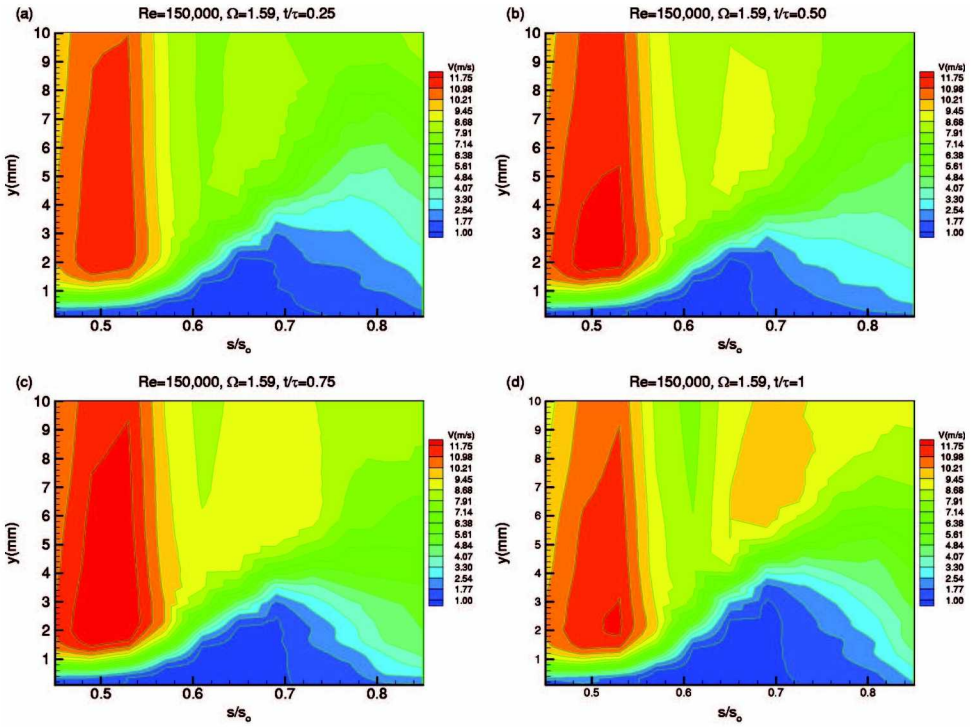

Fig. 15 Ensemble-averaged velocity contours along the suction surface for different s/s_0 with time t/τ as parameter for Ω=1.59 (S_R=160 mm), Re=150,000

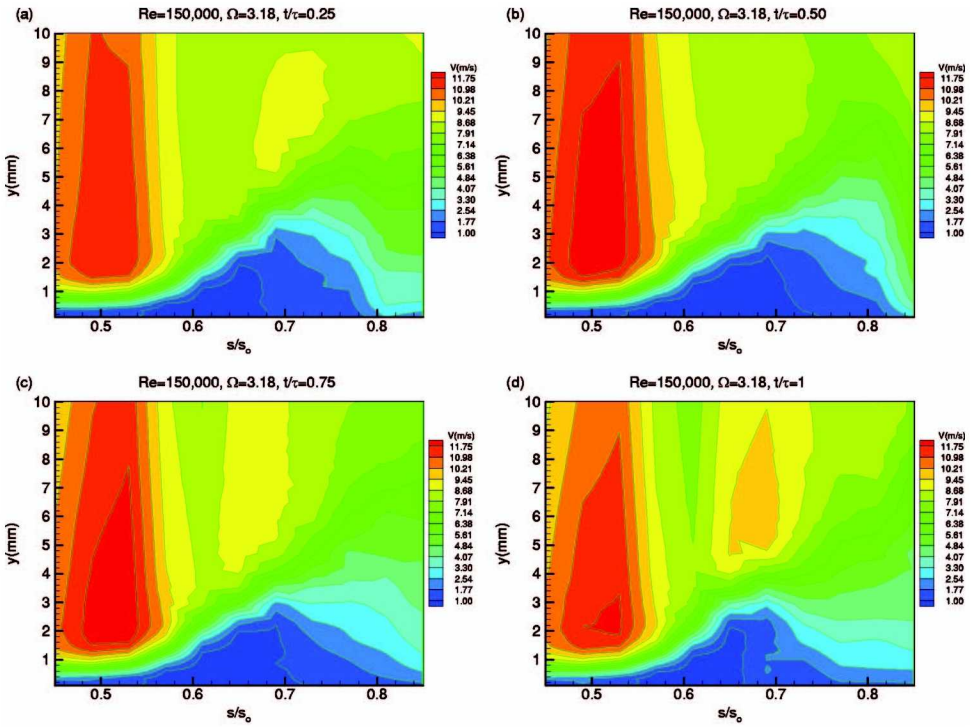

Fig. 16 Ensemble-averaged velocity contours along the suction surface for different s/s_0 with time t/τ as parameter for Ω=3.18 (S_R=80 mm), Re=150,000

$\langle \gamma_i(t_i) \rangle$ is integrated with respect to time to arrive at

$$\bar{\gamma} = \frac{1}{T} \int_{t=0}^{T} \langle \gamma_i(t_i) \rangle dt \tag{11}$$

Figure 17 shows the processing of instantaneous velocities.

Ensemble-Averaged Intermittency Distribution. Figure 18 presents the temporal-spatial contours of the ensemble-averaged intermittency distribution at three different lateral positions above the blade suction surface, y=1.341, 1.755, and 6.10 mm, for two reduced frequencies, Ω=1.59 and Ω=3.18. For better comparison of the effects of the impinging wake frequency, Fig. 18 exhibits

only the first three wakes. In this figure, the wakes with the highly vortical cores display intermittency values close to 0.6 indicating the transitional character of the boundary layer at the particular instant of time of wake impingement on the surface. Intermittency is approximately equal to zero outside the wake region near the leading edge, showing the nonturbulent behavior of the flow.

The wakes represented by narrow green strips pass through the turbine blade channel and periodically switch the boundary layer from laminar to turbulent and vice versa. Upstream of the separation bubble a pretransitional strip with an ensemble-averaged intermittency of $\gamma(t) \approx 0.5$ starting at $s/s_0 \approx 0.43$ and ending at $s/s_0 \approx 0.52$ separates the attached boundary layer from the bubble leading edge. At $s/s_0 \approx 0.52$, the visibility of the wake vanishes due to the interaction with the separation bubble. As Fig. 18 shows, the separation bubble starts at $s/s_0 \approx 0.52$ and extends up to $s/s_0 \approx 0.75$, thus occupying more than 24% of the suction surface and forming a large separation zone. At $s/s_0 \approx 0.75$, the intermittency field in Figure 18(*a*) displays an abrupt change in intermittency level, which indicates the start of a reattachment process. Once the wake passes over the separation zone, its signature reappears again as spots, with higher intermittency level (red) associated with becalmed zones (blue). Increasing Ω to 3.18, Fig. 18(*b*), causes an earlier mixing of the impinging wakes which results in widening the areas occupied by the wake vortical core, thus reducing the wake external region. Figure 18(*b*) suggests that further increase of Ω may lead to a complete degeneration of the deterministic periodic wake flow into a stochastic turbulence. Figures 18(*c*)–18(*f*) display the intermittency distributions at higher normal position from the blade surface. They are quite identical with Figs. 18(*a*) and 18(*b*) discussed above.

The intermittency distributions in Fig. 18 clearly show the unsteady nature of the boundary layer transition. In this form, however, they cannot quantitatively describe the complex unsteady transition, separation and reattachment process. To establish the basic relations essential for a quantitative description of the unsteady boundary layer transition, we resort to the fundamental study by Schobeiri and his coworkers [23] that deals with the physics of steady and unsteady wake development in a curved environment. The study clearly shows that the turbulence structure of the steady and unsteady wake flow is determined by the wake defect, which is a Gaussian function. Following the above study, we define a dimensionless parameter

$$\zeta = \frac{tU_w}{b} = \frac{ts_R}{\pi b} = \frac{\xi_2}{b} \text{ with } b = \frac{1}{\sqrt{\pi}} \int_{-\infty}^{+\infty} \Gamma d\xi_2 \tag{12}$$

Equation (12) relates the wake passing time t with the wake passing velocity in the lateral direction U_w, and the intermittency width b, with ξ_2 as the lateral distance from the wake center [23]. The intermittency width b is directly related to the wake width introduced by Schobeiri and his coworkers [7,12,23]. In an analogous way to find the defect function, we define the relative intermittency, Γ, as

$$\Gamma = \frac{\langle \gamma_i(t_i) \rangle - \langle \gamma_i(t_i) \rangle_{\min}}{\langle \gamma_i(t_i) \rangle_{\max} - \langle \gamma_i(t_i) \rangle_{\min}} \tag{13}$$

In the above equation, $\langle \gamma_i(t_i) \rangle$ is the time dependent ensemble-averaged intermittency function, which determines the transitional nature of an unsteady boundary layer. The intermittency $\langle \gamma_i(t_i) \rangle_{\max}$ exhibits the maximum intermittency value inside the wake vortical core. Finally, $\langle \gamma_i(t_i) \rangle_{\min}$ represents the minimum ensemble-averaged intermittency values outside the wake vortical core.

A representative relative intermittency function, Γ, is shown in Figs. 19(*a*)–19(*d*) for a frequency value of $\Omega = 1.59$ at lateral distances from the blade surface of $y = 0.858$, 0.996, 5.3, and 9.3 mm, with the dimensionless longitudinal distance s/s_0 as a parameter. The above distances are representative for intermittency distributions before, inside and outside the separation bubble over the entire suction surface. The symbols represent the experimental data. As seen for the reduced frequency of $\Omega = 1.59$, the measured relative intermittency functions follow very closely a Gaussian distribution, given by

$$\Gamma = e^{-\zeta^2} \tag{14}$$

with ζ as the nondimensionalized lateral length scale defined in Eq. (12). The slight deviation within and after the separation zone is due to a difficulty associated with capturing the maximum and minimum intermittencies. Using Eq. (14) as a generally valid intermittency relationship for unsteady wake flows, the intermittency function $\langle \gamma_i(t_i) \rangle$ is completely determined if additional information about the intermittency functions $\langle \gamma_i(t_i) \rangle_{\max}$ and $\langle \gamma_i(t_i) \rangle_{\min}$ are available. The distribution of $\langle \gamma_i(t_i) \rangle_{\max}$ and $\langle \gamma_i(t_i) \rangle_{\min}$ in the streamwise direction are plotted in Fig. 20 for Ω values of 1.59 and 3.18 on the suction surface. The distribution of $\langle \gamma_i(t_i)_{\max} \rangle$ corresponds to the condition when the wake, with its high turbulence intensity core, impinges on the plate surface. Once the wake has passed over the surface, the same streamwise location is exposed to a low turbulence intensity flow regime with an intermittency state of $\langle \gamma_i(t_i) \rangle_{\min}$, where no wake is present.

Figure 20 displays the striking features of $\langle \gamma(t) \rangle_{\max}$ and $\langle \gamma(t) \rangle_{\min}$. While for zero and moderate pressure gradients, the minimum intermittency $\langle \gamma_i(t_i) \rangle_{\min}$ distribution reveals a certain

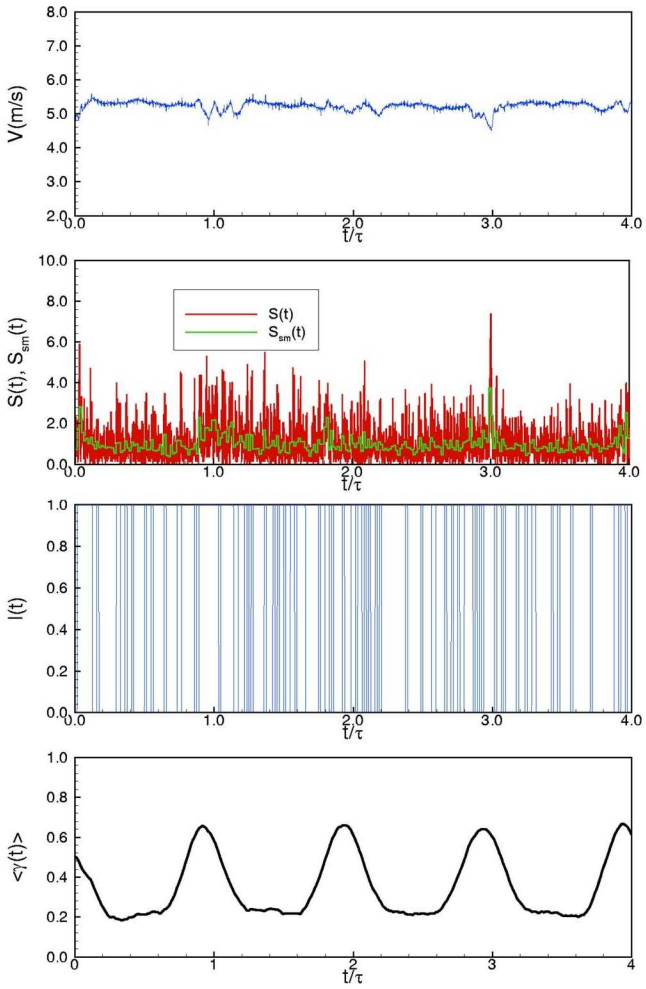

Fig. 17 Calculation of ensemble-averaged intermittency function from instantaneous velocities for $\Omega = 1.725$ at $y = 0.720$ mm

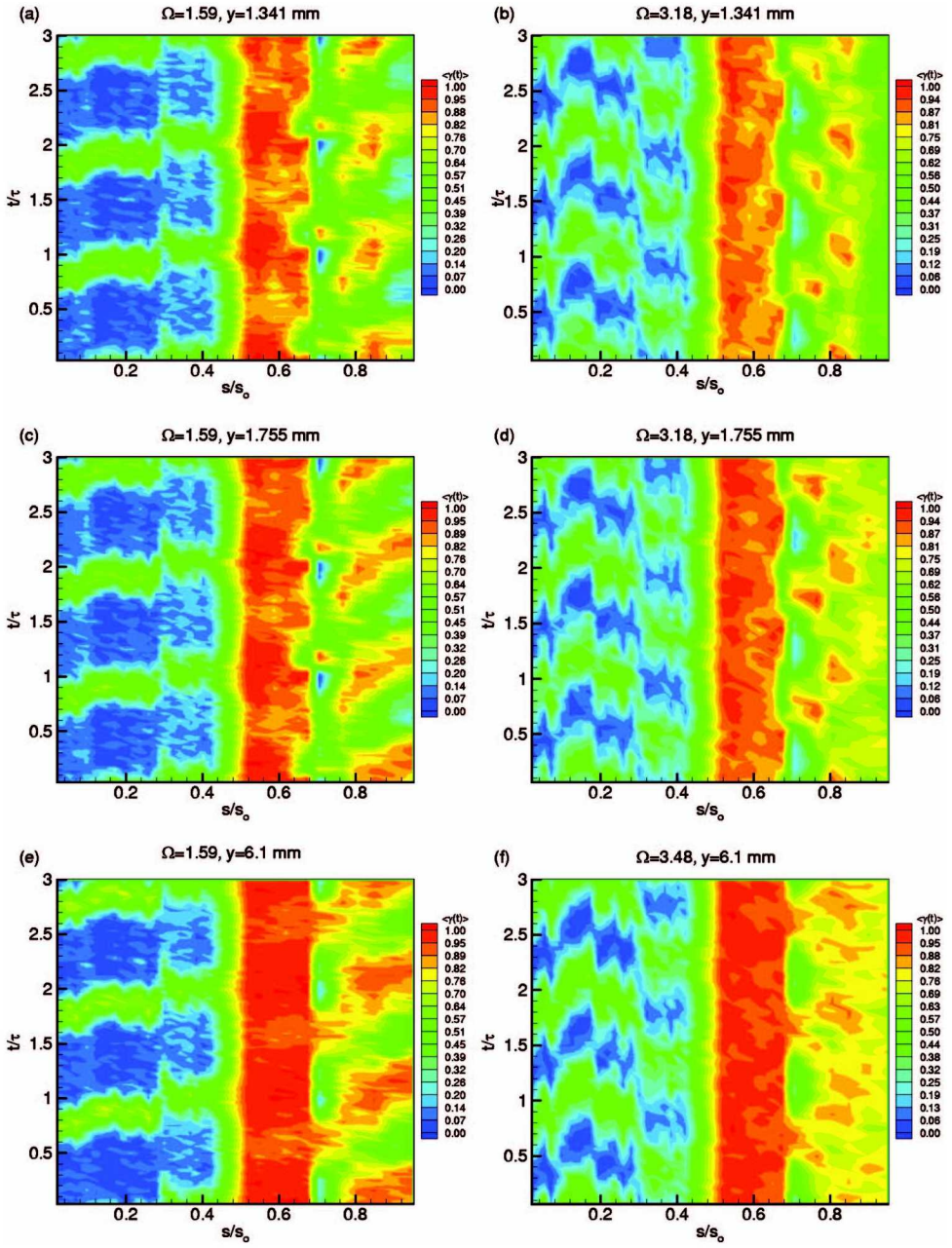

Fig. 18 Ensemble-averaged intermittency factor in the temporal-spatial domain at different *y* positions for $\Omega=1.59$ ($S_R=160$ mm) and $\Omega=3.18$ ($S_R=80$ mm)

similarity to the one described by the Emmons-Narasimha transition model [31], the present LPT-flow case with a strong negative pressure gradient associated with separation, $\langle\gamma_i(t_i)\rangle_{\min}$ exhibits a remarkably different course that occurs systematically and reproducibly for all Ω cases at all y positions over the blade surface. Upstream of the separation bubble, the course of $\langle\gamma(t)\rangle_{\min}$ with the value close to zero indicates a stable *nonturbulent* character of the boundary layer. A sharp increase in intermittency indicates the separation begins shortly before the pressure minimum (Fig. 4) has been reached. It is followed by a high intermittency region that covers the separation plateau (Fig. 4) and a steep decrease that is indicative of reattachment. The streamwise location of the intermittency minimum at $s/s_0\approx 0.7$ coincides with the end of the separation plateau. The following increase in intermittency is due to the steep positive pressure gradient that follows the constant pressure plateau. On the other hand, $\langle\gamma_i(t_i)\rangle_{\max}$ reveals a fundamentally different behavior. As Fig. 20 shows, the wake flow with an intermittency of $\langle\gamma_i(t_i)\rangle_{\max}\approx 0.8-0.9$ impinges on the blade surface. By convecting downstream, because of an extremely thin boundary layer, the wake turbulent fluctuations do not undergo a strong damping by the wall shear stress forces, as was observed in zero and moderate pressure gradient cases reported in Refs. [7,12].

Utilizing $\langle\gamma(t)\rangle_{\max}$ and $\langle\gamma(t)\rangle_{\min}$, the relative intermittency Γ is found to be described by a Gaussian distribution. This observation is in accord with the findings reported in Refs. [7,12], and very recently in Ref. [30] confirming the universal character of Γ. Considering the intermittency results of the current investigations and those reported above, it can be concluded that, in general, $\langle\gamma_i(t_i)\rangle_{\max}$ and $\langle\gamma_i(t_i)\rangle_{\min}$ are not only functions of reduced frequency, but they are also strongly influenced by the pressure gra-

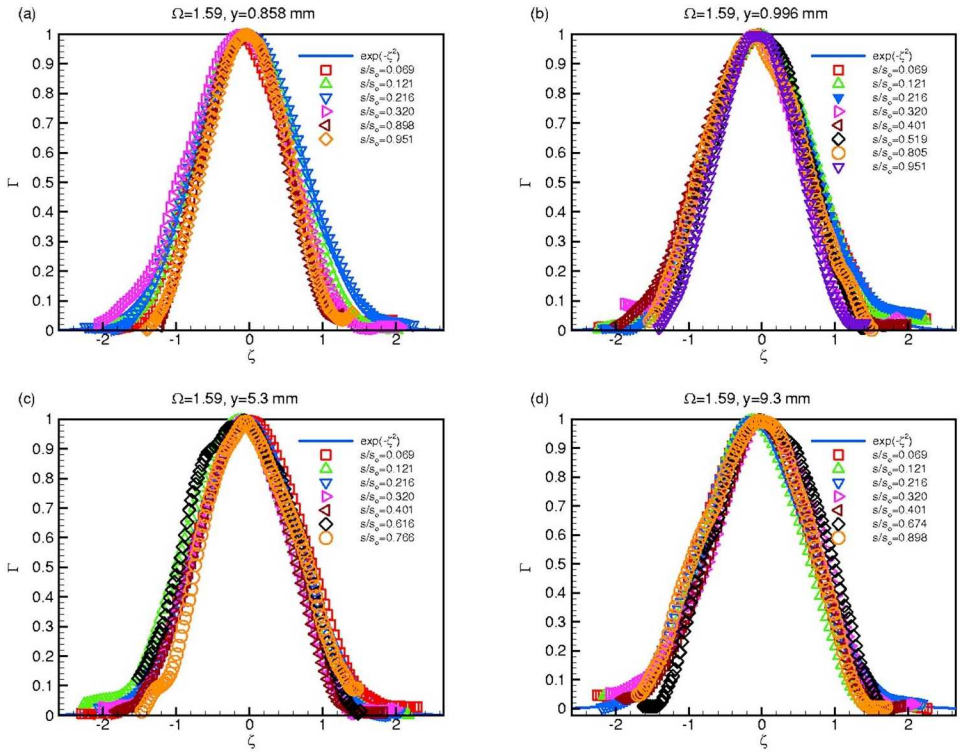

Fig. 19 Relative intermittency as a function of s/s_0 for unsteady frequency of Ω=1.59 (S_R =160 mm) at (*a*) *y*=0.858 mm, (*b*) *y*=0.996 mm, (*c*) *y*=5.3 mm, and (*d*) *y*=9.3 mm at Re =110,000

dient, turbulence intensity, Reynolds—and possibly Mach number, and surface roughness. This implies that neither $\langle \gamma_i(t_i) \rangle_{\min}$ nor $\langle \gamma_i(t_i) \rangle_{\max}$ have universal character.

Uncertainty Analysis

The Kline and McClintock [32] uncertainty analysis method was used to determine the uncertainty in the velocity after calibration and data reduction for the single-wire probe. The Kline and McClintock method determines the uncertainty with a 95% confidence level. The uncertainty in the velocity for the single-wire probe after the data reduction is given in Table 2. As shown, the uncertainty in the velocity increases as the flow velocity decreases. This is due to the pneumatic pressure transducer having a large uncertainty during calibration.

Conclusions

A detailed experimental study on the behavior of the separation bubble along the suction surface of a highly loaded LPT blade under periodic unsteady wake flow was presented. Varying the Reynolds number, one steady and two different unsteady inlet wake flow conditions with the corresponding passing frequencies, the wake velocity and the turbulence intensities were investigated by utilizing a large-scale, subsonic research facility. Periodic unsteady wake flow was established by translational motion of two parallel moving timing belts on which cylindrical rods were attached. The following conclusions were drawn.

Table 2 Uncertainty in velocity measurement for hot-wire probe

$\overline{V}$ (m/s)	3	5	12
$\omega\overline{V}/\overline{V}_0$(%)	5.78	2.41	1.40

(1) Slight changes of the pressure distribution occurred, while operating at the unsteady flow conditions. Increasing the Reynolds number from Re=110,000 to Re=150,000 has not brought major changes in steady state C_p distribution. However, the combination of higher Reynolds number with higher unsteady wake frequency introduced higher fluctuation kinetic energy into the boundary layer, which tends to reverse the separation tendency. C_p distribution clearly shows that the wake impingement with higher Reynolds number shortens the streamwise extent of the separation zone compared to the steady case.

(2) Detailed unsteady boundary layer measurement identified the onset and extent of the separation bubble as well as its behavior under the unsteady wake flow. Passing the wake flow with its highly turbulent vortical core over the separation region caused a periodic contraction and expansion of the separation bubble and a reduction of the separation bubble height. Increasing the passing frequency associated with a higher turbulence intensity further reduced the separation bubble height. It was observed that, by increasing the Reynolds number to 150,000, the leading edge and trailing edge of the separation bubble and, thus, the re-attachment point, moved further downstream to s/s_0=0.56 and s/s_0=0.788, respectively. Also, the size of the separation bubble was further reduced.

(3) Intermittency analysis of the current boundary layer experimental data with the flow separation determined the minimum, maximum, and the relative intermittency functions, $\langle \gamma_{\min} \rangle$, $-\langle \gamma_{\max} \rangle$, and Γ. The minimum intermittency function, $\langle \gamma_{\min} \rangle$, represented the boundary layer behavior when it is exposed to the wake external region (region between the turbulent wake strips). On the other hand, $\langle \gamma_{\max} \rangle$ describes the state of the boundary layer when it is subjected to the wake vortical core with its high turbulence level.

(4) The relative intermittency factor followed a Gaussian distribution confirming the universal character of the relative intermittency function. In contrast to the relative intermittency function Γ,

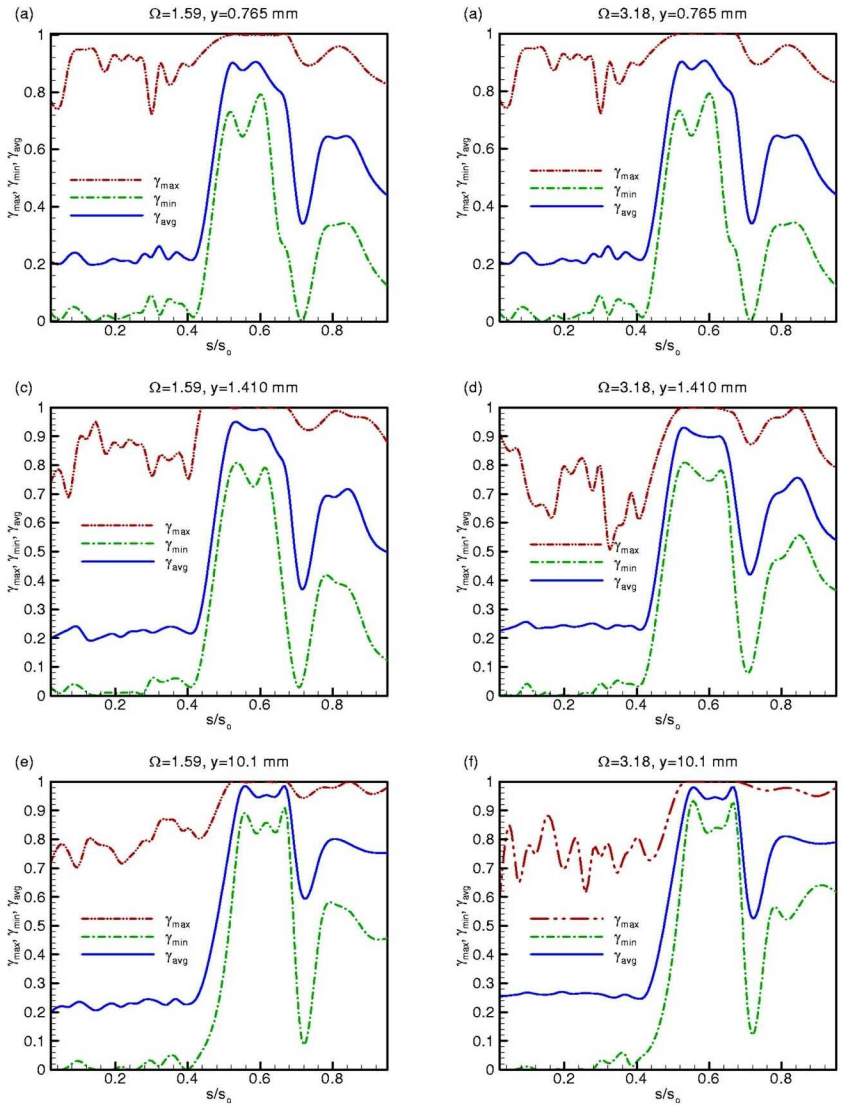

Fig. 20 Maximum, minimum, and time-averaged intermittency as a function of s/s_0 at different lateral positions for steady case $\Omega=0$ ($S_R=\infty$) and unsteady cases $\Omega=1.59$ ($S_R=160$ mm) and $\Omega=3.18$ ($S_R=80$ mm) at Re=110,000

the minimum as well as the maximum intermittency do not suggest to have a universal character. Several parameters, such as free-stream turbulence intensity, reduced frequency, surface roughness, Re number, and pressure gradient, are instrumental in affecting the pattern of these two intermittencies. Future studies need to incorporate these parameters.

Acknowledgment

The study presented is a part of an ongoing LPT-aerodynamics project executed by the NASA Glenn Research Center. The first two authors were supported by NASA Cooperative Agreement NCC3-793 monitored by Dr. David Ashpis. The support and the permission for publication are gratefully acknowledged. The authors also gratefully acknowledge Pratt & Whitney for providing the research community with the blade coordinates.

Nomenclature

b = intermittency wake width
c = blade chord
c_{ax} = axial chord
C_p = pressure coefficient, $C_p=(p_i-p_s)/(p_t-p_s)_{inl}$
C = threshold level
d_R = rod diameter
H_{12} = shape factor, $H_{12}=\delta_1/\delta_2$
h_m = maximum separation bubble height
$I(\mathbf{x},t)$ = indicator function
L_{SS} = suction surface length
M = number of samples
N = number of wake cycles
p_i = static pressure taps $i=1,..,48$
p_s, p_t = static, total pressure
Re_{LSS} = suction surface Reynolds number $\mathrm{Re}=L_{ss}V_{exit}/\nu$
s = streamwise distance from the leading edge of the blade
s_{md} = streamwise location of maximum separation bubble height
s_o = streamwise distance from the leading edge to the trailing edge of the blade
s_r = re-attachment point of the separation bubble from blade leading edge
s_s = start of the separation bubble at a streamwise distance from blade leading edge
$S(\mathbf{x},t)$ = criterion function

S_B = blade spacing
S_R = rod spacing
t = time
Tu = reference turbulence intensity
$\langle \mathrm{Tu} \rangle$ = ensemble-averaged turbulence intensity
U = belt translational velocity
v = fluctuation velocity
V = velocity
V_{ax} = axial velocity
V_{exit} = exit velocity
$\mathbf{x}$ = position vector
y = lateral distance from plate surface
$\alpha_{1,2}$ = cascade inlet, exit flow angles
γ = cascade stagger angle
$\bar{\gamma}$ = time-averaged intermittency
$\langle(\gamma)\rangle$ = ensemble-averaged intermittency
$\langle(\gamma)\rangle_{max}$ = maximum ensemble-averaged intermittency
$\langle(\gamma)\rangle_{min}$ = minimum ensemble-averaged intermittency
Γ = relative turbulence intermittency
ζ = nondimensional coordinate, y/b
ν = kinematic viscosity
ξ_2 = lateral distance from wake center
ρ = density of air
σ = cascade solidity, $\sigma = c/S_B$
τ = one wake-passing period
φ = flow coefficient, $\varphi = V_{ax}/U$
ψ_A = Zweifel coefficient
$\psi_A = 2\sin^2 \alpha_2(\cot \alpha_2 - \cot \alpha_1) S_B/c_{ax}$
Ω = reduced frequency $\Omega = (c/S_R)(U/V_{ax})$
$= (\sigma/\varphi)(S_B/S_R)$

References

[1] Pfeil, H., and Herbst, R., 1979, "Transition Procedure of Instationary Boundary Layers," ASME Paper No. 79-GT-128.
[2] Pfeil, H., Herbst, R., and Schröder, T., 1983, "Investigation of the Laminar Turbulent Transition of Boundary Layers Disturbed by Wakes," ASME J. Eng. Power, **105**, pp. 130–137.
[3] Orth, U., 1992, "Unsteady Boundary-Layer Transition in Flow Periodically Disturbed by Wakes," ASME Paper No. 92-GT-283.
[4] Schobeiri, M. T., and Radke, R. E., 1994, "Effects of Periodic Unsteady Wake Flow and Pressure Gradient on Boundary Layer Transition Along the Concave Surface of a Curved Plate," ASME Paper No. 94-GT-327.
[5] Schobeiri, M. T., Read, K., and Lewalle, J., 2003, "Effect of Unsteady Wake Passing Frequency on Boundary Layer Transition, Experimental Investigation and Wavelet Analysis," ASME J. Fluids Eng., **125**, pp. 251–266.
[6] Wright, L., and Schobeiri, M. T., 1999, "The Effect of Periodic Unsteady Flow on Boundary Layer and Heat Transfer on a Curved Surface," ASME J. Heat Transfer, **120**, pp. 22–33.
[7] Chakka, P., and Schobeiri, M. T., 1999, "Modeling of Unsteady Boundary Layer Transition on a Curved Plate under Periodic Unsteady Flow Condition: Aerodynamic and Heat Transfer Investigations," ASME J. Turbomach., **121**, pp. 88–97.
[8] Liu, X., and Rodi, W., 1991, "Experiments on Transitional Boundary Layers with Wake-Induced Unsteadiness," J. Fluid Mech., **231**, pp. 229–256.
[9] Schobeiri, M. T., Pappu, K., and Wright, L., 1995, "Experimental Study of the Unsteady Boundary Layer Behavior on a Turbine Cascade," ASME Paper No. 95-GT-435.
[10] Schobeiri, M. T., John, J., and Pappu, K., 1997, "Experimental Study on the Effect of Unsteadiness on Boundary Layer Development on a Linear Turbine Cascade," Exp. Fluids, **23**, pp. 303–316.
[11] Schobeiri, M. T., and Wright, L., 2003, "Advances in Unsteady Boundary layer Transition Research: Part I and II," Int. J. Rotating Mach., **9**(1), pp. 1–22.
[12] Schobeiri, M. T., and Chakka, P., 2002, "Prediction of Turbine Blade Heat Transfer and Aerodynamics Using Unsteady Boundary Layer Transition Model," Int. J. Heat Mass Transfer, **45**, pp. 815–829.
[13] Brunner, S., Fottner, L., and Schiffer, H.-P., 2000, "Comparison of Two Highly Loaded Turbine Cascade Under the Influence of Wake-Induced Transition," ASME Paper No. 2000-GT-268.
[14] Cardamone, P., Stadtmüller, P., Fottner, L., and Schiffer, H.-P., 2000, "Numerical Investigation of the Wake-Boundary Layer Interaction on a Highly Loaded LP Turbine Cascade Blade," ASME Paper No. 2002-GT-30367.
[15] Schulte, V., and Hodson, H. P., 1996, "Unsteady Wake-Induced Boundary Layer Transition in High Lift LP Turbines," ASME Paper No. 96-GT-486.
[16] Kaszeta, R., Simon, T. W., and Ashpis, D. E., 2001, "Experimental Investigation of Transition to Turbulence as Affected by Passing Wakes," ASME Paper No. 2001-GT-0195.
[17] Lou, W., and Hourmouziadis, J., 2000, "Separation Bubbles Under Steady and Periodic Unsteady Main Flow Conditions," ASME Paper No. 200-GT-270.
[18] Schröder, Th., 1989, "Measurements With Hot-Film Probes and Surface Mounted Hot Film Gages in a Multi-Stage Low Pressure Turbine," European Propulsion Forum, Bath, UK.
[19] Haueisen, V., Hennecke, D. K., and Schröder, T., 1997, "Measurements With Surface Mounted Hot Film Sensors on Boundary Layer Transition in Wake Disturbed Flow," AGARD-CP-598.
[20] Halstead, D. E., Wisler, D. C., Okiishi, T. H., Walker, G. J., Hodson, H. P., and Shin, H.-W., 1997, "Boundary Layer Development in Axial Compressors and Turbines: Part 3 of 4," ASME J. Turbomach., **119**, pp. 225–237.
[21] Schobeiri, M. T., and Öztürk, B., 2003, "On the Physics of the Flow Separation Along a Low Pressure Turbine Blade Under Unsteady Flow Conditions," ASME Paper No. 2003-GT-38917, ASME J. Fluids Eng., **127**, pp. 503–513.
[22] Schobeiri, M. T., and Öztürk, B., 2004, "Experimental Study of the Effect of the Periodic Unsteady Wake Flow on Boundary Layer Development, Separation, and Re-Attachment Along the Surface of a Low Pressure Turbine Blade," ASME J. Turbomach., **126**(4), pp. 663–676.
[23] Schobeiri, M. T., John, J., and Pappu, K., 1996, "Development of Two-Dimensional Wakes Within Curved Channels, Theoretical Framework and Experimental Investigation," ASME J. Turbomach., **118**, pp. 506–518.
[24] Hourmouziadis, J., 1989, "Blading Design for Axial Turbomachines," AGARD, Lecture Series LS-167.
[25] Eifler, J., 1975, "Zur Frage der freien turbulenten Strömungen, insbesondere hinter Ruhenden und bewegten Zylindern," Dissertation D-17, Technische Hochschule Darmstadt, Germany.
[26] Hedley, B. T., and Keffer, F. J., 1974, "Turbulent/Non-Turbulent Decisions in an Intermittent Flow," J. Fluid Mech., **64**, pp. 625–644.
[27] Antonia, R. A., and Bradshaw, P., 1971, Imp. College Aero. Rep. No. 71–04.
[28] Kovasznay, L. S. G., Kibens, V., and Blackwelder, R. F., 1970, J. Fluid Mech., **41**, p. 283.
[29] Bradshaw, P., and Murlis, J., 1973, Imp. College Aero. Tech. Note, No. 73–108.
[30] Schobeiri, M. T., 2005, "Intermittency Based Unsteady Boundary Layer Transition Modeling, Implementation Into Navier-Stokes Equations," ASME Paper No. GT2005–68375.
[31] Dhawan, S., and Narasimha, R., 1958, "Some Properties of Boundary Layer Flow During The Transition From Laminar to Turbulent Motion," J. Fluid Mech., **3**, pp. 418–436.
[32] Kline, S. J., and McKlintock, F. A., 1953, "Describing Uncertainties in Single-Sample Experiments," Mech. Eng. (Am. Soc. Mech. Eng.), **75**, pp. 3–8.